Random Walks of Cytoskeletal Motors in Open and Closed Compartments

Reinhard Lipowsky, Stefan Klumpp, and Theo M. Nieuwenhuizen*

Max-Planck-Institut für Kolloid und Grenzflächenforschung, 14424 Potsdam, Germany
(Received 18 November 2000; published 17 August 2001)

Random walks of molecular motors, which bind to and unbind from cytoskeletal filaments, are studied theoretically. The bound and unbound motors undergo directed and nondirected motion, respectively. Motors in open compartments exhibit anomalous drift velocities. Motors in closed compartments generate stationary nonequilibrium states with spatially varying densities of the motor concentrations and currents. "Traffic jams" on the filaments lead to a maximum of the motor current at an optimal motor concentration. Quantitative estimates based on experimental data for bound motors indicate that these transport phenomena are accessible to experiments.

Biological molecules, organelles, and cells constantly undergo riotous motion which may represent passive diffusion or active processes driven by chemical reactions [1]. One intriguing example for active transport is provided by the intracellular traffic of molecular motors along cytoskeletal filaments [2]. The movements of these motors involve several time regimes: (I) the molecular dynamics underlying the chemomechanical coupling, (II) the directed walks of the motors bound to the filaments, and (III) the random walks arising from many diffusional encounters between the motors and the filaments.

In this Letter, we address the long-time regime (III) and study its interrelation with the transport properties of the bound motors in regime (II). The latter properties have been measured for several types of motors [3–10]. Two of these motors, two-headed kinesin on microtubules [4] and myosin V on actin filaments [9], were found to walk via discrete steps with step sizes of 8 and 36 nm, respectively.

Regime (III) applies to the intracellular traffic which involves transport over tens of micrometers or even many decimeters as in the case of axons. The corresponding transport properties depend on the motor-filament interactions, on the arrangement of the filaments, and on the geometry of the confining membranes. Inspired by these biological processes, we study the transport of motors in open and closed compartments with immobilized filaments as shown in Fig. 1. In general, the filaments may be mobile as well [11] or may be assembled and disassembled [2] but these more complex processes will not be addressed here.

The directed walks of the bound motors can be characterized by a walking time Δt_b, which is the average time period between binding and unbinding. For all cytoskeletal motors studied so far, Δt_b was found to be of the order of a few seconds [5–10]. On time scales large compared to Δt_b, the motors undergo random walks which consist of alternating sequences of bound and unbound motor states. Such walks were previously discussed for unbounded geometries using scaling arguments [12].

In this Letter, we map the random walks of the molecular motors onto lattice random walks. This provides a general theoretical framework into which one can incorporate

(i) all transport properties of the bound motors as observed experimentally, (ii) the large difference between the bound and unbound diffusion coefficients, (iii) sticking probabilities for motor rebinding, and (iv) arbitrary motor-motor interactions. For unbounded geometries, some transport properties can be calculated analytically [13]. Here we focus on the confined systems displayed in Fig. 1 for which we describe two *generic* transport phenomena. In addition, we report results of Monte Carlo (MC) simulations for a specific parameter choice as appropriate for two-headed kinesin.

First, we study the motion of a "tracer" motor within open compartments as in Fig. 1(a)–1(c). Such a motor still advances parallel to the filament but with a reduced velocity. For the half space and the slab, the velocity decays for long times t as $\sim 1/t$ and $v \sim 1/t^{1/2}$, respectively. For an open tube, the velocity is reduced by a constant factor which depends on the radius of the tube. This reduction could be experimentally observed via fluorescent probes and single-particle tracking.

Second, for *closed* compartments as in Fig. 1(d), we find stationary nonequilibrium states with a motor concentration gradient between the two ends of the tube. This gradient leads to a diffusive backflow of the motors
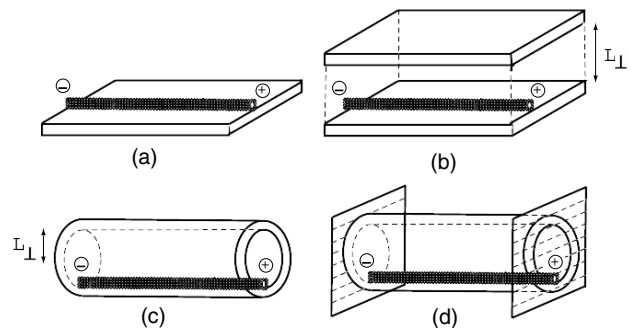
FIG. 1. Open and closed compartments with one filament (black rod) attached to the confining walls: (a) half space as used in [4–7,9,10], (b) slab, (c) open tube, and (d) closed tube. The motors are taken to move from the minus end of the filament to its plus end. The length scale $L_\perp$ denotes the thickness of the slab and the radius of the tube.

which balances the bound motor current along the filament. This balance is strongly affected by the hard-core repulsion (or mutual exclusion) between the motors: These interactions lead to "traffic jams" on the filaments even at relatively small motor concentrations. As a result of these jams, we find that the bound current exhibits a *maximum* at an *optimal* motor concentration.

In the presence of hard-core interactions, our models are new variants of driven lattice gases or exclusion processes. Related models have been previously studied for ionic conduction [14], nonequilibrium phase transitions [15,16], and macroscopic traffic flow [17].

Our Letter is organized as follows. First, we summarize the experimental results on bound motors and discuss the diffusion coefficient of unbound ones. We then define our random walk models, discuss the movement of single tracer motors in the different open compartments, and determine the density profiles of the motor concentrations and currents within closed tubes.

The experimental results for bound motors [3–10] are summarized in Table I. The walking time Δt_b and the walking distance Δx_b are related via $\Delta x_b = v_b \Delta t_b$ where v_b is the motor velocity along the filament. The walking time Δt_b depends on the overall ionic strength [5,10], on the presence of certain ions such as magnesium [C. Schmidt and M. Rief (private communication)], and on the filament roughness arising from adsorbed tau proteins [8] or from chemically altered tubulin [10].

The nondirected diffusive motion of the unbound motor, on the other hand, is governed by the diffusion coefficient D_{ub}. This coefficient is given by the Stokes-Einstein relation $D_{ub} = k_B T/(6\pi \eta R_{\text{hyd}})$ [1], and depends on the thermal energy $k_B T$, on the dynamic viscosity η of the solution, and on the effective hydrodynamic radius R_{hyd} of the motor particle. At room temperature, this leads to $D_{ub} = (\eta_w/\eta) \times (100 \text{ nm}/R_{\text{hyd}}) \times 2.4 \ \mu\text{m}^2/\text{s}$ with $\eta_w \simeq 0.9$ mPa s ($\equiv cP$) as appropriate for water [18].

We will now map the random walks of the motors onto lattice random walks. The parameters of our lattice models can be chosen in such a way that the lattice random walks exhibit the same diffusion coefficient D_{ub}, walking time Δt_b, bound state velocity v_b, and bound state diffusion coefficient D_b as the real motors.

In our models, the motor particle moves on a cubic lattice with lattice constant ℓ. For simplicity, the filament is taken to consist of one protofilament which corresponds to a one-dimensional line of binding sites [19]. The motor can adsorb onto a filament binding site from n_{ad} adjacent nonfilament sites with $n_{ad} = 4$ and 3 for a filament in solution and attached to a wall, respectively.

Away from the filament, the hopping rates between any two nearest neighbor sites are equal to $1/6\tau$ where the time scale τ for the unbound motor is given by $\tau = \ell^2/6D_{ub}$. When the motor moves to a filament binding site, it adsorbs with sticking probability π_{ad}. Once the motor is bound to the filament, it is governed by a different time scale denoted by τ_b: it can make a forward or backward step to a neighboring filament site with rates α/τ_b and β/τ_b, respectively, or unbind from it to an adjacent nonfilament site with rate $\epsilon/6\tau_b$. The dwell probability $\gamma \equiv 1 - \alpha - \beta - n_{ad}\epsilon/6$ defines the mean dwell time $\tau_{dw} = \tau_b \gamma/(1 - \gamma)$ and the mean *step time* $\tau_s \equiv \tau_{dw} + \tau_b = \tau_b/(1 - \gamma)$.

The unbinding probability ϵ is determined by the walking time Δt_b via $\Delta t_b/\tau_b = (6/n_{ad} - \epsilon)/\epsilon$. The bound state velocity and diffusion coefficient are given by $v_b = (\bar{\alpha} - \bar{\beta})\ell/\tau_b$ and $D_b = [\bar{\alpha} + \bar{\beta} - (\bar{\alpha} - \bar{\beta})^2]\ell^2/2\tau_b$ with $\bar{\alpha} \equiv \alpha/(\alpha + \beta + \gamma)$ and $\bar{\beta} \equiv \beta/(\alpha + \beta + \gamma)$.

In the MC simulations reported here, we focus on two-headed kinesin, for which we ignore backward steps [6] choosing $\beta = 0$. This leads to $\tau_b = [1 - 2D_b/\ell v_b]\ell/v_b$ and, via the entries in the first row of Table I, to $\tau_b = 5.9$ ms. The measured values of v_b and D_b are recovered for $\alpha = 0.4975$, $\gamma = 0.4987$, and $\epsilon = 0.0075$ which also implies $\tau_s = 11.8$ ms and $\Delta t_b/\tau_s = 133$. In addition, the bulk diffusion coefficient is taken to be $D_{ub} = 4 \ \mu\text{m}^2/\text{s}$ which implies $\tau = \tau_b/1341$, and the sticking probability $\pi_{ad} = 1$.

Now, consider an open compartment with one long filament attached to its surface as in Fig. 1. The motor concentration is small and the motor-motor interactions can be ignored. The corresponding time evolution for the displacement x of a single motor is shown in Fig. 2.

The simplest open compartment is a half-space geometry as in Fig. 1(a). The filament has coordinates $(x, y = 0, z = 0)$. When the motor unbinds from this filament, it can explore the half space $z > 0$ in front of the surface. The velocity v of the motor parallel to the filament is equal to v_b for its bound state but vanishes in its unbound state. For long times t, the probability density $\mathcal{P}_\perp(y, z, t)$

TABLE I. Filament repeat distance ℓ, bound state velocity v_b, bound state diffusion coefficient D_b, walking distance Δx_b, and walking time Δt_b as measured for high ATP concentration and low load. The motors in [6,9,10] were attached to beads; the motors in [7] had no tails. The bounds for myosin V follow from the low probability for backward steps.

	ℓ (nm)	v_b (nm/s)	D_b (nm^2/s)	Δx_b (μm)	Δt_b (s)
Two-headed kinesin [6]	8	680	1360		
Two-headed kinesin [7]	8	710	2200	2	2.6
One-headed kinesin [7]	8	140	44 000	0.84	6.1
Dynein [10]	8	422		2.6	
Two-headed myosin V [9]	36	$\lesssim 360$		1.6	$\gtrsim 4.5$
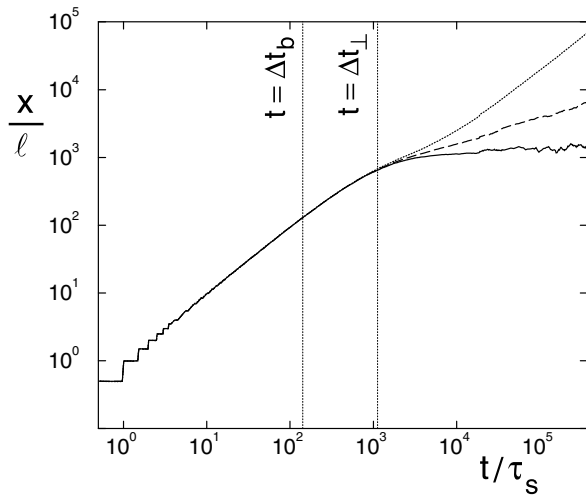
FIG. 2. Simulation data for motor displacement x as a function of time t in units of the filament repeat distance ℓ and the mean step time τ_s. The bottom, middle, and top lines are for the half space, slab, and open tube, respectively. The slab thickness and the tube radius are $L_\perp = 500\ell$.

for the perpendicular motor coordinates has the scaling form $\mathcal{P}_\perp(y, z, t) = \Phi(y/t^{1/2}, z/t^{1/2})/t$ where the factor $1/t$ arises from the normalization $\int dy\, dz\, \mathcal{P}_\perp(y, z, t) = 1$. Thus, the probability $\mathcal{P}_b$ for the motor's bound state decays as $\mathcal{P}_b \approx c_1 \pi_{ad} \Delta t_b / t$ and its velocity decays as $v = v_b \mathcal{P}_b \approx c_1 \pi_{ad} \Delta x_b / t$ for large t. Our MC data give $c_1 \simeq 0.50$ while the analytical solution for the unbounded space suggests $c_1 = 3/2\pi \simeq 0.48$. This implies that the motor displacement x grows very slowly with time as $x(t) - x(t_o) \approx c_1 \pi_{ad} \Delta x_b \ln(t/t_o)$ for large t.

Within the slab, the parallel displacement of the motor first exhibits the same time evolution as in the half space until the motor is likely to diffuse back to the filament after being reflected from the second surface which has a separation $L_\perp$ from the first one. This happens after the diffusion time $\Delta t_\perp \equiv (2L_\perp)^2/2D_{ub}$. For later times, the motor velocity decays as $v(t) \approx c_2 \pi_{ad} \Delta x_b / (\Delta t_\perp t)^{1/2}$ and its displacement evolves as $x(t) \approx 2c_2 \pi_{ad} \Delta x_b (t/\Delta t_\perp)^{1/2}$; our MC data give $c_2 \simeq 1.16$.

Next, the motor is placed in an open cylindrical tube with radius $L_\perp$ as in Fig. 1(c). In this case, the velocity initially decreases as in the other geometries until the motor is confined by the walls of the tube. It then alternates between bound and unbound states with average lifetime Δt_b and $\Delta t_\perp$, respectively. Thus, for $t \gg \Delta t_\perp$, the velocity attains the finite value $v_{\mathrm{eff}} = \Delta x_b / [\Delta t_b + \Delta t_\perp / c_3]$ which behaves as $v_{\mathrm{eff}} \approx c_3 \pi_{ad} \Delta x_b / \Delta t_\perp$ for large $L_\perp$. Our MC data yield $c_3 \simeq 1.92$.

Finally, consider a closed tube as in Fig. 1(d). Both the tube and the filament now have the longitudinal length $L_\|$. Because of the confining walls, the motors cannot step backwards at the minus nor forwards at the plus end of the filament. For all other sites, we use the same hopping probabilities as before. Since the filament strongly attracts the motors, it becomes overcrowded or "jammed" even for

relatively small motor concentrations. Thus, in order to obtain reliable densities for the bound motors, one has to take the hard-core repulsion (or mutual exclusion) of the motors into account [20].

Within the closed tube, the active transport of the motors along the filament generates a concentration gradient between the two ends of the tube. Any gradient, $\nabla\rho_{ub}$, of the unbound motor concentration ρ_{ub} induces a diffusive current $J_{ub} \equiv -D_{ub}\nabla\rho_{ub}$ which acts to reduce the gradient. Therefore, the motor density will adjust in such a way that this diffusive current J_{ub} balances the bound current J_b along the filament.

The balance between bound and unbound currents is delicate, however, since the motors constantly bind to and unbind from the filament, and the rebinding is strongly reduced by traffic jams on the filaments. As long as the number N of motors is sufficiently small, the filament still provides many unoccupied binding sites and each diffusing motor, which collides with the filament, rebinds to it with the "bare" sticking probability π_{ad}. Therefore, each unbound motor can diffuse back only over a certain distance before it is recaptured by the filament. This leads to density profiles $\rho_b = \rho_b(x)$ of the bound motors which decay rapidly as one moves away from the plus end; see Fig. 3 for $N = 40$.

For large N, on the other hand, the whole filament is overcrowded or jammed, and each unbound motor has to undergo many collisions with the filament before it can reattach to it. As a result, the bound motor density $\rho_b(x)$ is close to its maximal value over the whole length of the tube as shown in Fig. 3 for $N = 250$.

Thus, as one increases the overall motor concentration $\rho = N/\pi L_\perp^2 L_\|$, the filament starts to become overcrowded at the plus end, and this traffic jam then spreads towards the minus end with increasing ρ. At intermediate values of ρ, one has a density profile which interpolates between the two limiting cases; see Fig. 3 with
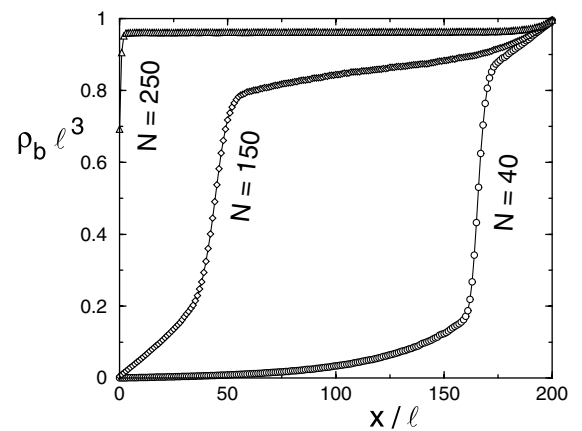
FIG. 3. Closed tube: Local concentrations ρ_b of bound motors as a function of the coordinate x parallel to the filament in units of ℓ. The three curves correspond to different values of the total number N of motors. The tube has length $L_\| = 200\ell$ and radius $L_\perp = 25\ell$; its plus end is at $x = L_\|$.
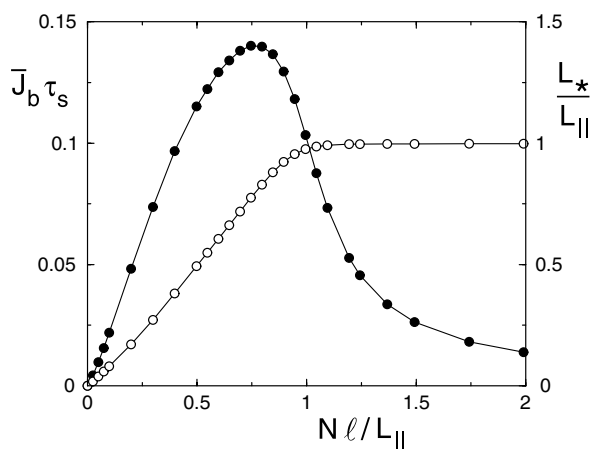
FIG. 4.   Average current $\bar{J}_b$ of bound motors (full circles) and "jam" length L_* (open circles) as a function of the total motor number N. The parameters τ_s and $L_\parallel = 200\ell$ are the mean step time and the filament length, respectively. The tube geometry is the same as in Fig. 3. The current $\bar{J}_b$ attains its maximal value for $N \simeq 150$; for this case, the jam has spread out to $L_* \simeq 0.77L_\parallel$; see Fig. 3.

$N = 150$ [21]. One simple way to characterize the density profiles is via the "jam" length L_* which is defined by $\rho_b(x = L_*)\ell^3 = 1/2$; see Fig. 4.

In addition to the density profiles $\rho_b(x)$, we also determined the profiles $J_b = J_b(x)$ of the bound currents which are maximal in the boundary region between the jammed and the "free" part of the filament. The overall transport along this filament can be characterized by the average current $\bar{J}_b \equiv \int dx \, J_b(x)/L_\parallel$. As shown in Fig. 4, this quantity exhibits a maximum as a function of the motor particle number N. For small N, the average current grows linearly with N; for large N, on the other hand, the current decreases again since the average velocity of each bound motor is strongly reduced by the overcrowding of the filament. For the chosen tube volume $\pi L_\perp^2 L_\parallel = 3.9 \times 10^5 \ell^3$, the maximal current occurs for $N \simeq 150$ motor particles. Using the repeat distance $\ell = 8$ nm for microtubules, this motor particle number corresponds to a kinesin concentration of $\simeq 3 \ \mu$M.

If one starts with a random distribution of motors within the closed tube, the qualitative features of the density profiles shown in Fig. 3 are observed after about 5×10^5 MC steps. Since the time for one MC step is $\tau = \tau_s/2680 \simeq 4.4 \times 10^{-6}$ s, this self-organization process is completed after a couple of seconds. If each bound kinesin motor in the maximal current state hydrolyzes one adenosine triphosphate (ATP) per step time τ_s, the total number of ATP molecules consumed during this time corresponds to about 20% of a 1 mM ATP solution [22].

In summary, we have shown that the random walks of cytoskeletal motors exhibit anomalous drift velocities in open compartments and self-organized concentration gradients in closed ones. The latter gradients arise from a balance between bound and unbound motor currents which is a generic feature of the systems studied here [19]. Such a balance may also be effective for the motor traffic within biological cells which is, however, more difficult to estimate since the unbound motors can stick to other "particles" within the cytosol. Very recently, Nedelec et al. [23] used fluorescent microscopy to measure the concentration profiles of kinesins within arrays of microtubules. The same experimental method may be used in order to observe the profiles displayed in Fig. 3.

---

*Permanent address: Institute for Theoretical Physics, University of Amsterdam, Valckenierstraat 65, 1018 XE Amsterdam, The Netherlands.

[1] H. C. Berg, Random Walks in Biology (Princeton University Press, Chichester, 1993).

[2] B. Alberts et al., Molecular Biology of the Cell (Garland, New York, 1994), 3rd ed.

[3] J. Howard, A. J. Hudspeth, and R. D. Vale, Nature (London) 342, 154 (1989).

[4] K. Svoboda, C. Schmidt, B. Schnapp, and S. Block, Nature (London) 365, 721 (1993).

[5] R. D. Vale et al., Nature (London) 380, 451 (1996).

[6] M. J. Schnitzer and S. M. Block, Nature (London) 388, 386 (1997).

[7] Y. Okada and N. Hirokawa, Science 283, 1152 (1999).

[8] B. Trinczek, A. Ebneth, E.-M. Mandelkow, and E. Mandelkow, J. Cell. Sci. 112, 2355 (1999).

[9] A. Mehta et al., Nature (London) 400, 590 (1999).

[10] Z. Wang and M. Sheetz, Biophys. J. 78, 1955 (2000), used bead motility assays with ~60 motors per bead.

[11] F. J. Nedelec, T. Surrey, A. C. Maggs, and S. Leibler, Nature (London) 389, 305 (1997).

[12] A. Ajdari, Europhys. Lett. 31, 69 (1995).

[13] Th. M. Nieuwenhuizen, S. Klumpp, and R. Lipowsky (to be published).

[14] S. Katz, J. Lebowitz, and H. Spohn, J. Stat. Phys. 34, 497 (1984).

[15] J. Krug, Phys. Rev. Lett. 67, 1882 (1991).

[16] R. Zia, L. Shaw, B. Schmittmann, and R. Astalos, Comput. Phys. Commun. 127, 23 (2000).

[17] T. Antal and G. Schütz, Phys. Rev. E 62, 83 (2000).

[18] For $\eta = \eta_w$, $D_{ub} \gg D_b$, compare Table I, but $D_{ub} \sim 1/\eta$ can be strongly reduced by additional solutes.

[19] We have also studied filaments with several protofilaments and systems containing networks of filaments.

[20] If one included cargo beads with a radius R, they would occupy a lattice volume $\sim(R/\ell)^3$ and thus enhance the exclusion effects on the filaments.

[21] In the low density regime, $\rho_b(x) \sim \exp[x/L_\rho]$. The length scale L_ρ depends on the total binding energy ΔE of one motor particle to the filament and is given by $L_\rho \sim \exp[-\Delta E/(k_b T)]D_{ub}L_\perp^2/(v_b \ell^2)$.

[22] In order to sustain these states for an extended period of time, one could couple the compartment to a reservoir of ATP molecules, e.g., via semipermeable walls which are permeable for ATP but impermeable for the motors.

[23] F. Nedelec, T. Surrey, and A. C. Maggs, Phys. Rev. Lett. 86, 3192 (2001).